SARLiquid: Through-package Liquid Leakage Detection based on mmWave SAR Imaging

Zhanjun Hao[1*], Changlong Zhao[1], Yimiao Sun[2]
Yuejiao Wang[3], Guowei Wang[3], Yuan He[2]
[1]Northwest Normal University, [2]School of Software and BNRist, Tsinghua University, [3]Lanzhou University
{haozhj,202421162063}@nwnu.edu.cn,sym21@mails.tsinghua.edu.cn
{wyuejiao2024,wanggw2024}@lzu.edu.cn,heyuan@tsinghua.edu.cn

Abstract

Liquid leakage detection is critical for product quality and user safety, yet existing methods require line-of-sight (LoS) or direct contact with the liquid, or could even introduce additional health or safety risks. In this paper, we propose SARLiquid, a novel mmWave-based through-package liquid leakage detection method. SARLiquid leverages mmWave signals to see through packaging and identify leakage by reconstructing mmWave images. We employ synthetic aperture radar (SAR) technique to enhance imaging resolution and tame multipath effects. We also develop a dedicated algorithm to calibrate the discontinuous phase in SAR imaging results, and propose a deep learning model for liquid leakage detection and liquid identification. We implement SARLiquid and evaluate it across a wide range of scenarios. Results show that SARLiquid achieves average accuracies above 93% for both liquid leakage detection and liquid identification, 14.70% and 9.98% higher than the baselines, respectively.

CCS Concepts

• **Computer systems organization → Embedded and cyber-physical systems**.

Keywords

Liquid, mmWave, Imaging, SAR

ACM Reference Format:
Zhanjun Hao[1*], Changlong Zhao[1], Yimiao Sun[2], Yuejiao Wang[3], Guowei Wang[3], Yuan He[2]. 2026. SARLiquid: Through-package Liquid Leakage Detection based on mmWave SAR Imaging. In *Workshop on Network and Operating System Support for Digital Audio and Video (NOSSDAV '26), April 4–8, 2026, Hong Kong, Hong Kong.* ACM, New York, NY, USA, 7 pages. https://doi.org/10.1145/3798065.3798078

NOSSDAV '26, Hong Kong, Hong Kong

ACM ISBN 979-8-4007-2534-0/26/04
https://doi.org/10.1145/3798065.3798078

1 Introduction

Liquid goods are usually packaged in modern industrial production and distribution for convenient transport, storage, and retail handling [1, 4, 10, 17, 28]. However, leakage from sealed packages often occurs during these processes, leading to potential economic loss and microbial growth. More critically, for high-proof alcohols and other volatile liquids, leakage may pose severe safety risks (*e.g.*, fire or harmful vapor release). Therefore, reliable liquid leakage detection is essential to ensure product quality and consumer safety [12, 23, 30].

Existing research has explored a range of methods for liquid leakage detection. Vision-based methods [6, 14] extract visual features of leakage in target regions, while RFID-based methods [7] deploy tags in sensing areas to infer leakage based on the changes in tags' dielectric properties. However, these methods either require an unobstructed line of sight (LoS) or rely on direct contact with leaked liquid, which is difficult to satisfy when liquid goods are sealed in packages. Although X-ray imaging can see through packaging without requiring LoS or direct contact, its ionizing radiation raises significant health and safety concerns.

In this paper, we propose SARLiquid, a novel through-package liquid leakage detection method based on mmWave imaging. At its core, SARLiquid exploits mmWave signals with inherent penetrability to see through packaging. Materials (*e.g.*, liquid and bottle) inside a package exhibit different permittivities and thus introduce distinct responses to mmWave signals [3]. These differences will manifest in reconstructed mmWave images, enabling SARLiquid to identify and localize leaked liquid. However, realizing the idea is non-trivial and presents several technical challenges:

First, mmWave propagation inside packaged environments undergoes complex reflections and multipath effects, which could significantly distort reconstructed images and degrade detection accuracy. Second, permittivity differences among materials inside the package will induce discontinuous phase variations, which impair image quality. Third, practical deployments should accommodate diverse liquids, yet their features may be subtle in reconstructed images, making reliable liquid identification difficult.

Zhanjun Hao[1*], Changlong Zhao[1], Yimiao Sun[2]
Yuejiao Wang[3], Guowei Wang[3], Yuan He[2]

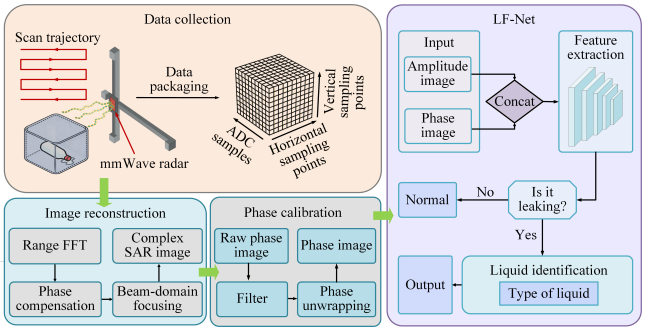

Figure 1: Overview of SARLiquid.

To address these challenges, SARLiquid incorporates the following core designs. First, we employ synthetic aperture radar (SAR) technique[1] along with a phase compensation method to improve spatial resolution and tame multipath effects inside enclosed environments. Second, we develop a dedicated phase calibration algorithm to unwrap the discontinuous phase and suppress noise in reconstructed images. Third, we propose a deep learning model for joint leakage detection and liquid identification.

Our contribution can be summarized as follows:

1) We propose SARLiquid, a novel method for through-package liquid leakage detection. We disclose the propagation model for mmWave signals in packaged scenarios and establish the relationship between liquid leakage and its features in mmWave images.

2) We design the mmWave imaging pipeline tailored for through-package leakage detection and address key challenges, including multipath effect, discontinuous phase variations, and joint leakage detection and liquid identification.

3) We implement SARLiquid and evaluate it across a wide range of packaging scenarios. Results show that SARLiquid achieves average accuracies above 93% for both leakage detection and liquid identification, 14.70% and 9.98% higher than the baseline, respectively.

2 SARLiquid Design

Fig. 1 provides an overview of SARLiquid. First, SARLiquid uses a commercial mmWave radar to scan the target along a predefined 2D trajectory, synthesizing a dense virtual array and collecting reflected signals. It then reconstructs SAR amplitude and phase images, in which leakage appears as unique energy anomalies and phase variations. Next, SARLiquid applies a phase calibration algorithm to denoise the phase image and correct phase discontinuities. Finally, the calibrated RGB phase and amplitude images are fed into LF-Net for joint leakage detection and liquid identification.

[1]SAR synthesizes a much larger effective antenna aperture by coherently combining echoes collected as the sensing device moves, achieving high-resolution sensing with a physically small antenna [8, 21, 31].

2.1 Signal Propagation Model

To characterize how leakage manifests in SAR images, we first model signal propagation in through-package scenarios.

In such scenarios, the received reflected mmWave signals consist of multiple components traveling along different paths. The i-th component can be expressed as [16]:

$$S_i = A_i \cdot e^{j\Phi_i}, \tag{1}$$

where A_i and Φ_i denote the amplitude and phase of the i-th path, respectively. Both are determined by the propagation distance, material attenuation, and the reflection/transmission coefficients along the path.

Next, we analyze these propagation paths under both the leakage and non-leakage scenarios, respectively.

Non-leakage scenario. As illustrated in Fig. 2(a), under the non-leakage scenario, the liquid remains fully contained within the container, and the received signal is dominated by three primary propagation paths:

1) Path A: The signal is reflected by the far inner surface of the packaging box, denoted as $R_{p_{out}}$.

2) Path B: The signal passes the packaging box and is reflected by the container's outer surface, denoted as $R_{c_{out}}$.

3) Path C: The signal penetrates the packaging box and the container, and is reflected by the liquid surface.

Among these paths, *Path C* is particularly important because it directly interacts with the liquid. Its amplitude and phase can be expressed as

$$\begin{aligned} A_3 &= S_0 G_t G_r T_{a\to p}^2 T_c R_l e^{-2(\alpha_p d_p + \alpha_c d_c)}, \\ \Phi_3 &= 2k\left(d_p + d_c\right) + 2\angle T_{a\to p} + \angle T_c + \angle R_l, \end{aligned} \tag{2}$$

where S_0 is the transmitted signal power; G_t and G_r are the transmit and receive antenna gains; $T_{a\to p}$ is the transmission coefficient at the air-packaging interface [26]; T_c denotes the overall transmission coefficient through the container interfaces (*i.e.*, $T_{a\to c}$ and $T_{l\to c}$); and R_l is the reflection coefficient at the liquid surface. α_p and α_c are the attenuation coefficients of the packaging box and container, respectively; d_p and d_c are their thicknesses; k is the wavenumber; and $\angle T_c$ and $\angle R_l$ are the phase shifts introduced by transmission and reflection at the container and liquid interfaces. Other paths can be formulated similarly, differing mainly in the reflection interfaces and corresponding attenuation terms.

Leakage scenario. As shown in Fig. 2(b), under the leakage condition, the liquid level in the container decreases, and the leaked liquid spreads to the bottom of the package. This introduces two additional propagation paths: *Path C′*, reflected from the region above the liquid level, and *Path D*, reflected from the leaked liquid at the package bottom:

1) Path C′: The signal penetrates the packaging box and the container, then is reflected by the inner surface of the container ($R_{c_{in}}$) in the region where the liquid has receded.

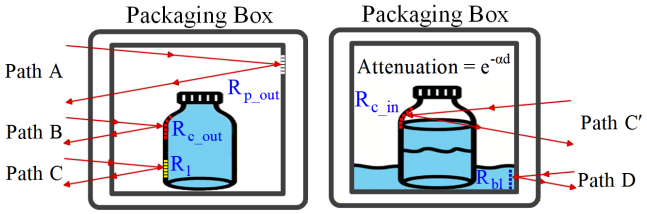

(a) Non-leakage (b) Leakage

Figure 2: Signal propagation model.

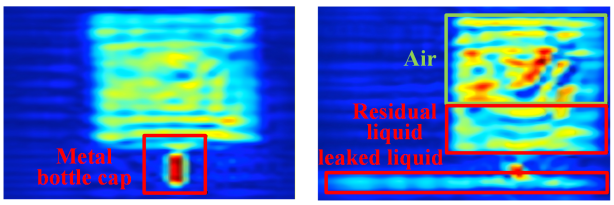

(a) W/o leakage (b) W/ Leakage

Figure 3: Comparison of w/o leakage and w/ leakage.

2) Path D: The signal is directly reflected by the leaked liquid surface through the packaging box. The corresponding amplitude and phase are

$$A_4 = S_0 G_t G_r T_{a\to p}^2 R_{bl} e^{-2\alpha_p d_p}, \\ \Phi_4 = 2k \cdot d_p + 2\angle T_{a\to p} + \angle R_{bl}\,, \tag{3}$$

where R_{bl} is the reflection coefficient of the leaked liquid, and $\angle R_{bl}$ denotes the phase shift introduced by it.

2.2 Imaging Mapping and Leakage Analysis

Image reconstruction. SAR imaging reconstructs the spatial distribution of scatterers by coherently integrating reflected signals collected over each synthetic aperture. Based on the signal propagation model in §2.1, the received signal at each aperture position is the coherent superposition of contributions from all propagation paths:

$$S_{total}\,(t,x,y) = \sum_{i=1}^{N} S_i\,, \tag{4}$$

where $N = 3$ in the non-leakage scenario and increases to $N = 5$ under the leakage scenario.

To form a focused SAR image, we adopt a standard FMCW-SAR reconstruction pipeline, including range-domain transformation, wavenumber-domain phase compensation, and inverse spatial transformation [29]. After compensating for phase distortions introduced by multilayer propagation, we reconstruct the complex SAR image as

$$f(x,y) = \mathrm{FFT}_{2D}^{-1}\left[\mathrm{FFT}_{2D}[S(x',y')] \cdot e^{-jz\sqrt{4k^2-k_x^2-k_y^2}}\right], \tag{5}$$

where k is the wavenumber and (k_x, k_y) are the spatial-frequency components along azimuth dimensions. This operation refocuses scattered energy to its true spatial location.

We obtain the SAR amplitude image by normalizing the power of reflected signals and mapping it to pixel intensity: $I(x,y) = |f(x,y)|^2/|f_{\max}|^2$, which can then visualize the relative reflection strength across the imaging plane.

Leakage analysis Based on the signal propagation model and the SAR reconstruction procedure described above, liquid leakage can be inferred based on two features in the reconstructed images:

1) Energy anomaly. Leakage substantially reshapes the spatial energy distribution because liquids typically exhibit much higher permittivity than air. Externally, leaked liquid spreads along the package bottom and forms an additional reflective interface (*Path D*), introducing a localized high-intensity region in the SAR amplitude image (Fig. 3(b)[2]). Internally, the drop in liquid level introduces a medium discontinuity along the propagation path: the receded, air-filled region experiences lower attenuation and thus appears brighter, whereas the remaining liquid region incurs higher absorption and exhibits reduced intensity. Together, these effects yield an energy anomaly for indicating the leakage.

2) Phase variation. In addition to amplitude changes, the permittivity difference between air and liquid also leads to distinct phase responses. Since electromagnetic waves propagate at different velocities in different media, leakage-induced changes in the propagation medium alter the effective optical path length, resulting in phase shifts along the corresponding paths. In the reconstructed phase image, these shifts manifest as discontinuities and/or specific texture patterns at the liquid interface to highlight the leakage.

2.3 Phase Calibration

While combining amplitude and phase images can ensure a reliable leakage detection, practical deployments should accommodate diverse liquids, which requires liquid identification. Liquid identification, however, hinges on finer and more stable phase features, yet the raw phase image is impacted by speckle noise, multipath interference, and wrapping discontinuities, as shown in Fig. 4(a1). To recover more accurate phase images, we develop a dedicated phase calibration algorithm.

First, we use the SAR amplitude image to guide spatial smoothing of the phase image. This strategy exploits the structural consistency between the two modalities to suppress speckle noise while preserving sharp phase edges around leakage regions. Second, to mitigate background multipath, we apply notch filtering in the frequency domain to remove low-frequency interference [19] and isolate leakage-related

[2]Here, we take a vertical deployment as an example, but SARLiquid can function well under diverse container deployments (detailed in §3.3 and Fig. 9(b).

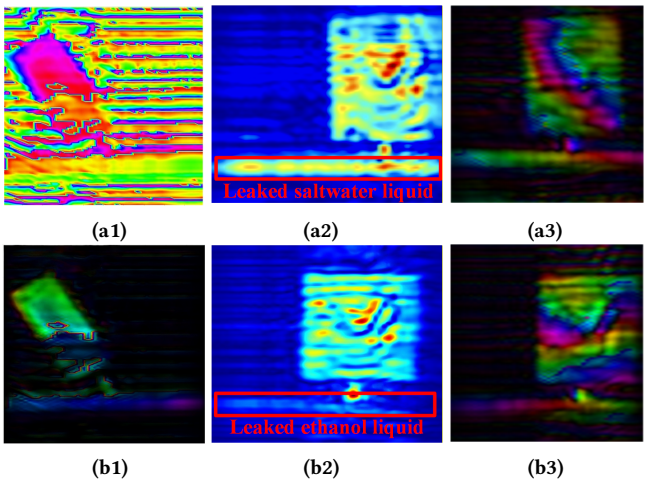

Figure 4: Comparison of amplitude and phase images. (a1) Phase image w/o calibration; (b1) Phase image w/ calibration; (a2) Amplitude image of saltwater; (b2) Amplitude image of ethanol; (a3) Phase image of saltwater; (b3) Phase image of ethanol.

high-frequency details. Finally, to resolve the phase ambiguity within $(-\pi, \pi]$, we implement a DCT-based least-squares phase unwrapping algorithm. By solving the Poisson equation via the discrete cosine transform, we efficiently recover a continuous absolute phase field, making the phase features more distinguishable for liquid classification.

To demonstrate the effectiveness of our phase calibration algorithm, we conduct a group of experiments[3]. We employ the proposed algorithm to calibrate the image of the ethanol leakage. As shown in Fig. 4(b1), the calibrated phase image exhibits a smoother and more continuous phase field while preserving the structural boundaries of the leakage region, in clear contrast to the raw phase image in Fig. 4(a1). This result confirms that our calibration effectively suppresses noise and corrects phase discontinuities without blurring leakage-relevant edge information.

We further quantify the improvement using three metrics: Peak Signal-to-Noise Ratio (PSNR), Phase Gradient Variance (PGV), and Phase Continuity Index (PCI). Results show that phase calibration improves PSNR by over 13 dB on average, indicating effective noise suppression. PGV, which reflects phase smoothness, improves by 78.16%, demonstrating reduced phase fluctuations. PCI increases by 11.99%, confirming the enhanced phase continuity. Overall, the calibration well recovers the absolute phase distribution, which could significantly improve the accuracy of liquid identification.

2.4 LF-Net

Input data. To fully exploit distinct physical responses of different materials, SARLiquid forms a 6-channel input tensor including RGB amplitude and phase images.

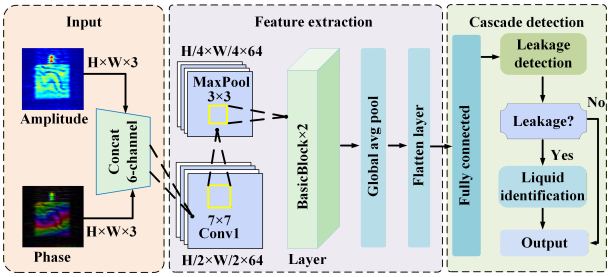

Figure 5: LF-Net network architecture.

On one hand, leakage introduces a new reflection path (*i.e.*, *Path D* in §2.1), which typically appears as a high-intensity region near the package bottom in the amplitude image (Fig. 4(a2) and (b2)). The intensity of this region correlates with the liquid's permittivity, with higher-permittivity liquids producing stronger responses. On the other hand, different liquids have distinct refractive indices and absorption coefficients, which affect the effective path length and multipath interference. As shown in Fig. 4(a3) and (b3) , these differences manifest as characteristic textures and fringes in the phase images. With both amplitude and phase features, LF-Net can learn to identify liquid while detecting leakage.

Network architecture. Fig. 5 illustrates the architecture of LF-Net. It is built on a modified ResNet-18 backbone, where the first convolutional layer is expanded to accept the 6-channel input. The backbone extracts a shared feature representation that captures both spatial energy cues (from amplitude) and fine-grained texture cues (from phase). This feature vector is then fed into two cascaded branches: *1) Leakage detection branch*, a binary classifier that predicts whether leakage occurs based on the anomaly features defined in §2.2; and *2) Liquid identification branch*, a multi-class classifier that predicts the liquid type and is activated only when leakage is detected.

3 Evaluation

3.1 Experimental Setup

Hardware and software. Fig. 6 illustrates the hardware setup of SARLiquid. We build SARLiquid on a commercial mmWave radar (Texas Instruments IWR1843BOOST [22]) operating over 77-81 GHz. The radar is mounted on a guide rail and driven by a set of stepper motors to follow a "snake" scanning trajectory (orange solid line in the top-right subfigure of Fig. 6). This trajectory synthesizes a 104×18 grid of virtual aperture positions (horizontal $\times$ vertical) for SAR imaging. We develop a dedicated graphical user interface (GUI) in MATLAB R2022a to control the guide rail and collect radar data. We implement LF-Net with Python 3.12 and

[3]The experimental dataset and setup are the same as those detailed in §3.1

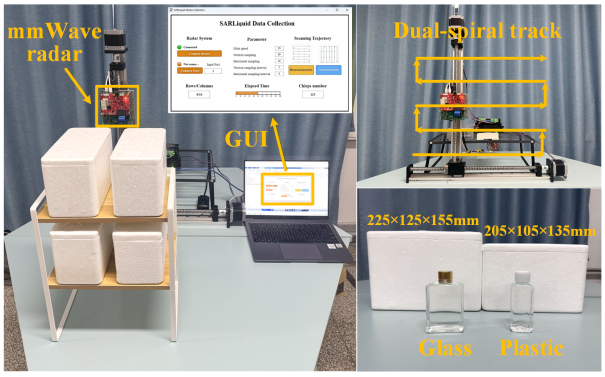

Figure 6: Experimental scenario and deployment.

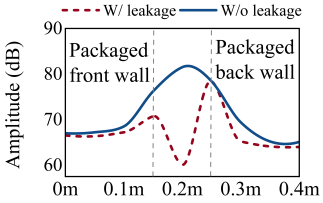

Figure 7: Range profiles of the baseline.

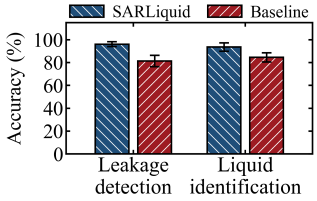

Figure 8: Overall performance comparison.

CUDA 12.1. All algorithms run on a laptop equipped with an Intel i7-1365HX CPU and an NVIDIA RTX 4060 GPU.

Dataset. We construct our dataset using four common liquids with different permittivities: water, saltwater, glycerin, and ethanol. For each liquid, we collect mmWave images under different conditions, including leakage state, container material (*e.g.*, glass *vs.* plastic), and other variables, yielding 2,040 samples in total. We split the dataset into training, validation, and test sets with a 70%/15%/15% ratio.

Baseline. For performance comparison, we implement a baseline that analyzes mmWave signals without SAR imaging. Specifically, the baseline collects reflected mmWave signals at multiple distances from the package. Then, similar to many existing methods [2, 13, 25], the baseline applies wavelet denoising for multipath suppressing and extracts a set of signal features (*i.e.*, kurtosis, peak position, peak ratio, and signal energy), which are further fed into a SVM model for joint leakage detection and liquid identification. We collect 7,500 samples to train and evaluate the baseline.

The rationality behind this baseline is illustrated in Fig. 7. Without leakage, the liquid-filled container forms a relatively uniform dielectric medium, yielding a single broad reflection peak as the distance varies. When leakage occurs, the liquid distribution inside the package changes and introduces additional reflections and attenuation, leading to destructive interference and a multiple-peak waveform.

3.2 Overall Performance

We evaluate SARLiquid and the baseline using 5-fold cross-validation, with results shown in Fig. 8. Specifically, SARLiquid achieves 96.05% accuracy for leakage detection, outperforming the baseline by 14.70%. For liquid identification, SARLiquid reaches 93.57% accuracy, which is 9.98% higher than that of the baseline. The performance of the baseline is largely limited by spatial resolution and strong multipath interference. In contrast, SARLiquid achieves high accuracy across because 2D SAR provides higher-resolution imaging results and better suppresses multipath effects.

3.3 Impacting Factors

Impact of sensing distance. First, we evaluate SARLiquid by varying the distance between the radar and the package from 155 mm to 185 mm, with a 10 mm step. For leakage detection, Fig. 9(a) shows only a modest performance degradation as distance increases. Even at 185 mm, all metrics (*i.e.*, precision, recall, accuracy, and F1-score) are above 0.94. For liquid identification, Fig. 10(a) also shows a slight accuracy drop as the distance increases. Nevertheless, the average identification accuracy remains above 93%, and it stays above 86% at 185 mm. These results demonstrate the robustness of SARLiquid within this operating range.

Impact of container deployment. We next evaluate the robustness of SARLiquid under different container deployments. Specifically, we consider three deployments: vertical, tilted, and horizontal. As shown in Fig. 9(b), leakage detection performs best in the tilted deployment. We attribute this to the smaller contact area between the container and the leaked liquid at the package bottom, which makes the leakage-induced reflection more dominant in the received signal. As the contact area increases (*e.g.*, horizontal and vertical deployments), the performance slightly degrades. Fig. 10(b) shows a similar trend for liquid identification, where the tilted deployment also achieves higher accuracy.

Impact of container material. We evaluate SARLiquid with two common container materials: glass and plastic. For leakage detection, SARLiquid remains highly robust. As shown in Fig. 9(c), all metrics remain above 0.92 for both materials, indicating that leakage-induced anomalies can be reliably captured regardless of container material. For liquid identification, Fig. 10(c) shows that SARLiquid also maintains stable performance across both materials. The slight performance degradation seen in glycerol and ethanol is mainly due to their low permittivities.

Impact of container shape. Besides material properties, container shape may also introduce variability in reflected mmWave signals. To evaluate its impact, we evaluate SARLiquid with two typical container shapes: rectangular and square. As shown in Fig. 9(d), all metrics exceed 0.91 for the two

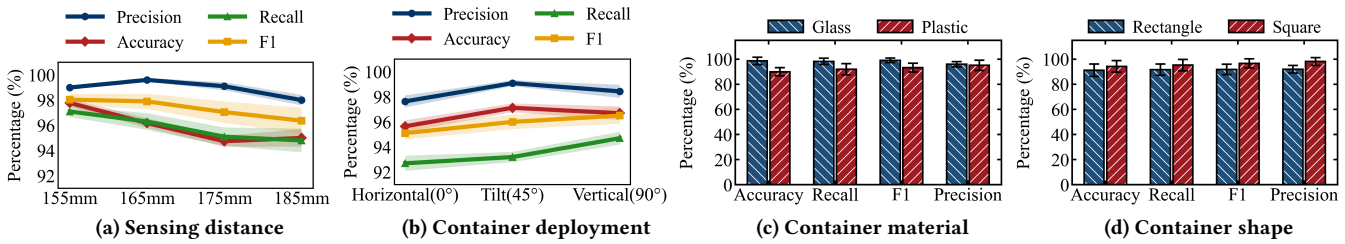

(a) Sensing distance (b) Container deployment (c) Container material (d) Container shape

Figure 9: Performance of leak detection under different impacting factors.

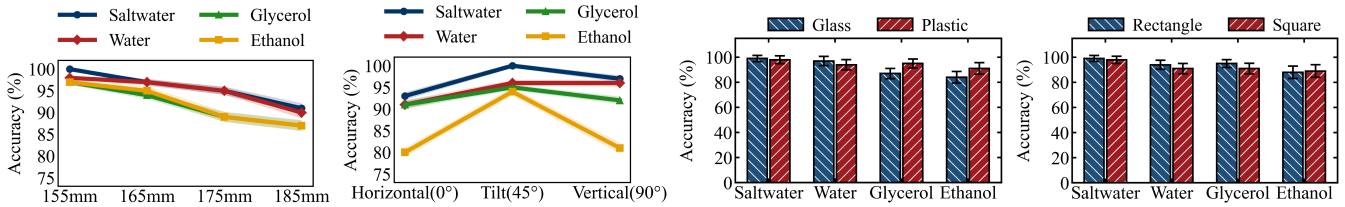

(a) Sensing distance (b) Container deployment (c) Container material (d) Container shape

Figure 10: Performance of liquid identification under different impacting factors.

shapes. This indicates that leakage detection is largely insensitive to container shape. For liquid identification, Fig. 10(d) shows that the accuracy gap between the two shapes is within 5% for all four liquids, suggesting SARLiquid's robustness to the variation of container shape.

4 Related Work

mmWave sensing has attracted extensive research [5, 9, 20]. For mmWave imaging, existing works mainly focus on reconstructing the target surface geometry. For instance, Song et al. [18] use reflection-intensity images to capture facial brightness differences for masked face authentication. Hao et al. [8] perform static gesture recognition by analyzing target contours in intensity images. Wang et al. [24] exploit metasurface reflections to increase spatial diversity and use diffusion models to generate higher-resolution images. Regmi et al. [15] apply phase compensation and compressed sensing to handle non-uniform sampling, and then use cGANs for 3D pose prediction.

Different from those works, SARLiquid adopts mmWave imaging to deal with the core challenges of liquid leakage detection in through-package scenarios.

5 Discussion

Robustness and scalability. Different materials inside the package exhibit distinct mmWave responses due to their permittivity differences. Based on this principle, SARLiquid can be easily extended to other liquids beyond those evaluated and can potentially identify other materials in the package.

Besides, SARLiquid does not produce false positives for underfilled but non-leaking containers, since leakage detection mainly depends on reflections from liquid accumulated at the package bottom. However, accuracy may degrade for micro-leakage cases, which may require finer-grained algorithms and we leave this for future work.

Time consuming. In the current implementation, SARLiquid requires about one hour to complete a full round of scanning and imaging. This latency can be significantly reduced by using higher-resolution radar hardware [11] or adopting sparse-sampling algorithms [27].

6 Conclusion

This paper presents SARLiquid, a novel through-package liquid leakage detection approach with a commercial mmWave radar. We disclose the propagation model for mmWave signals in packaged scenarios and address a series of practical challenges. Extensive experiments across diverse conditions demonstrate that SARLiquid achieves accurate joint leakage detection and liquid identification, with average accuracies above 93%. We envision SARLiquid as a practical solution for modern industrial production and distribution.

7 Acknowledgement

The work was supported by National Natural Science Foundation of China under Grants 62262061 and 62425207, Major Science and Technology Special Program of Gansu Province 23ZDGA009, and Central Government Guided Local Science and Technology Development Fund Project 25ZYJA007.

References

[1] Kecheng An, Qian Zhang, and Elaine Kwong. 2021. Viscocam: Smartphone-based drink viscosity control assistant for dysphagia patients. *Proc. of ACM IMWUT*.

[2] Dingyue Cao, Yuxiang Lin, Geng Ren, Yi Gao, and Wei Dong. 2022. MmLiquid: Liquid Identification Using mmWave. In *Proc. of Springer CWSN*.

[3] Yande Chen, Chongzhi Xu, Kexin Li, Jia Zhang, Xiuzhen Guo, Meng Jin, Xiaolong Zheng, and Yuan He. 2024. Wireless sensing for material identification: A survey. *IEEE Communications Surveys & Tutorials* 27, 3 (2024), 1598–1617.

[4] Ashutosh Dhekne, Mahanth Gowda, Yixuan Zhao, Haitham Hassanieh, and Romit Roy Choudhury. 2018. Liquid: A wireless liquid identifier. In *Proc. of ACM MobiSys*.

[5] Laura Dodds, Tara Boroushaki, Kaichen Zhou, and Fadel Adib. 2025. Non-Line-of-Sight 3D Object Reconstruction via mmWave Surface Normal Estimation. In *Proc. of ACM MobiSys*.

[6] Mina Fahimipirehgalin, Emanuel Trunzer, Matthias Odenweller, and Birgit Vogel-Heuser. 2021. Automatic Visual Leakage Detection and Localization from Pipelines in Chemical Process Plants Using Machine Vision Techniques. *Engineering* 7, 6 (2021), 758–776.

[7] Junchen Guo, Ting Wang, Yuan He, Meng Jin, Chengkun Jiang, and Yunhao Liu. 2019. TwinLeak: RFID-based Liquid Leakage Detection in Industrial Environments. In *Proc. of IEEE INFOCOM*.

[8] Zhanjun Hao, Ruidong Wang, Jianxiang Peng, and Xiaochao Dang. 2023. Static Hand Gesture Recognition Based on Millimeter-Wave Near-Field FMCW-SAR Imaging. *Electronics* 12, 19 (2023).

[9] Yuan He, Yimiao Sun, and Xiuzhen Guo. 2025. RF Computing: A New Realm of IoT Research. *Journal of Computer Science and Technology* 40, 4 (2025), 1–16.

[10] Yongzhi Huang, Kaixin Chen, Yandao Huang, Lu Wang, and Kaishun Wu. 2021. Vi-liquid: unknown liquid identification with your smartphone vibration. In *Proc. of ACM MobiCom*.

[11] Ltd. Huawei Technologies Co. 2025. *ASN850 Millimeter Wave Sensing Radar Product Specification*. Retrieved February 16, 2026 from https://e.huawei.com/cn/products/wireless/microwave/asn850-radar

[12] Zhaohui Li, Wei Luo, Yongmin Zhang, Jianxi Chen, Yuanchao Shu, and Yaoxue Zhang. 2024. ASLiquid: Non-Intrusive Liquid Counterfeit Identification with Your Earphones. In *Proc. of ACM SenSys*.

[13] Yumeng Liang, Anfu Zhou, Huanhuan Zhang, Xinzhe Wen, and Huadong Ma. 2021. FG-LiquID: A Contact-less Fine-grained Liquid Identifier by Pushing the Limits of Millimeter-wave Sensing. *Proc. of ACM IMWUT*.

[14] Chengang Lyu, Yage Liu, Xuekai Wang, Yuxin Chen, Jie Jin, and Jiachen Yang. 2022. Visual Early Leakage Detection for Industrial Surveillance Environments. *IEEE Transactions on Industrial Informatics* 18, 6 (2022).

[15] Hem Regmi, Moh Sabbir Saadat, Sanjib Sur, and Srihari Nelakuditi. 2021. SquiggleMilli: Approximating SAR Imaging on Mobile Millimeter-Wave Devices. *Proc. of ACM IMWUT*.

[16] Mark A. Richards, James A. Scheer, and William A. Holm. 2010. *Principles of Modern Radar: Basic principles*. The Institution of Engineering and Technology.

[17] Fei Shang, Panlong Yang, Yubo Yan, and Xiang-Yang Li. 2022. LiqRay: Non-invasive and fine-grained liquid recognition system. In *Proc. of ACM MobiCom*.

[18] Wenfan Song, Weiye Xu, Jianwei Liu, Yuanqing Zheng, Xinhuai Wang, Xian Xu, and Jinsong Han. 2026. Anti-Spoofing and Mask-Supported Face Authentication Using mmWave Without On-Site Registration. *IEEE Transactions on Dependable and Secure Computing* 23, 1 (2026).

[19] Yimiao Sun, Yuan He, Jiacheng Zhang, Xin Na, Yande Chen, Weiguo Wang, and Xiuzhen Guo. 2023. BIFROST: Reinventing WiFi Signals Based on Dispersion Effect for Accurate Indoor Localization. In *Proc. of ACM SenSys*.

[20] Yimiao Sun, Yuan He, Yang Zou, Jiaming Gu, Xiaolei Yang, Jia Zhang, and Ziheng Mao. 2025. A Survey of mmWave Backscatter: Applications, Platforms, and Technologies. *Comput. Surveys* 57, 9 (2025), 1–36.

[21] Yimiao Sun, Qunyan Zhou, Yulong Chen, Jiaming Gu, Qiang Cheng, and Yuan He. 2026. Metasurface-Enabled Multi-Target WiFi Sensing. *IEEE Transactions on Mobile Computing* 25, 3 (2026), 3985–3997.

[22] Texas Instruments. [n. d.]. *AWR1843BOOST and IWR1843BOOST Single-Chip mmWave Sensing Solution User's Guide (Rev. B)*. https://www.ti.com/tool/AWR1843BOOST

[23] Ju Wang, Jie Xiong, Xiaojiang Chen, Hongbo Jiang, Rajesh Krishna Balan, and Dingyi Fang. 2017. TagScan: Simultaneous target imaging and material identification with commodity RFID devices. In *Proc. of ACM MobiCom*.

[24] Yida Wang, Yu Lu, Yuxuan Zhou, Yifei Shen, Lili Qiu, Zeyuan Lai, Yi-Chao Chen, Hao Pan, Juntao Zhou, Dian Ding, Mei Wang, Guangtao Xue, and Qian Zhang. 2025. High-resolution mmWave Imaging using Metasurface and Diffusion. In *Proc. of ACM MobiSys*.

[25] Zhu Wang, Yifan Guo, Zhihui Ren, Wenchao Song, Zhuo Sun, Chao Chen, Bin Guo, and Zhiwen Yu. 2024. LiqDetector: Enabling Container-Independent Liquid Detection with mmWave Signals Based on a Dual-Reflection Model. *Proc. of ACM IMWUT*.

[26] Chenshu Wu, Feng Zhang, Beibei Wang, and K. J. Ray Liu. 2020. mSense: Towards Mobile Material Sensing with a Single Millimeter-Wave Radio. *Proc. of ACM IMWUT*.

[27] Shuxian Wu, Li Ding, Ping Li, Yinwei Li, Lin Chen, and Yiming Zhu. 2020. Millimeter-Wave SAR Sparse Imaging With 2-D Spatially Pseudorandom Spiral-Sampling Pattern. *IEEE Transactions on Microwave Theory and Techniques* 68, 11 (2020).

[28] Binbin Xie, Jie Xiong, Xiaojiang Chen, Eugene Chai, Liyao Li, Zhanyong Tang, and Dingyi Fang. 2019. Tagtag: Material sensing with commodity RFID. In *Proc. of ACM SenSys*.

[29] Muhammet Yanik and Murat Torlak. 2018. Millimeter-Wave Near-Field Imaging with Two-Dimensional SAR Data. In *Proc. of SRC Techcon*.

[30] Shichao Yue and Dina Katabi. 2019. Liquid testing with your smartphone. In *Proc. of ACM MobiSys*.

[31] Jia Zhang, Rui Xi, Yuan He, Yimiao Sun, Xiuzhen Guo, Weiguo Wang, Xin Na, Yunhao Liu, Zhenguo Shi, and Tao Gu. 2023. A Survey of mmWave-Based Human Sensing: Technology, Platforms and Applications. *IEEE Communications Surveys Tutorials* 25, 4 (2023), 2052–2087.